

The study of the gluon distribution function and reduced cross section behavior using the proton structure function

B.Rezaei* and G.R.Boroun†

Physics Department, Razi University, Kermanshah 67149, Iran

(Dated: June 24, 2020)

We present a set of formulas to extract the gluon distribution function and the reduced cross section from the proton structure function and its derivatives with respect to $\ln Q^2$ in the next-to-next-to-leading order of the perturbative theory at low x based on a hard pomeron exchange. The behavior of the DIS reduced cross section studied and compared with the experimental data, also these behaviors controlled by the nonlinear and higher twist corrections at low Q^2 . These results were augmented by including an additional higher-twist term in the description of the nonlinear correction. This additional term, modified nonlinear correction, improves the description of the reduced cross sections significantly at low values of Q^2 . Our calculations show a good agreement with the DIS experimental data throughout the low values of x . We discuss, furthermore, how this behavior can be determine the reduced cross section with respect to the proton parameterization at high- y values. These results within the next-to-next-to-leading order approximation at very low x can be applied in the LHeC and FCC-eh regions for analyses of ultra-high energy processes. The resulting predictions for σ_r suggest that further corrections are required for Q^2 less than about 3 GeV^2 .

Introduction

The gluon distribution in hadrons at small Bjorken x play a vital role in our understanding of the deep-inelastic scattering (DIS) and our predictions for new physics at the Large Hadron Collider (LHC) in ultra-high energy processes. It is important to know the gluon distribution inside a hadron at small x because gluons are expected to be dominant in this region. The gluons couple only through the strong interaction. Consequently the gluons cannot be measured directly in the DIS. Indeed, the gluon density is much higher than of charged partons and the photoabsorption will be dominated by the boson-gluon fusion (BGF) $\gamma^* p \rightarrow q\bar{q}$ [1].

The high-luminosity LHC program would be uniquely complemented by the proposed Large Hadron electron Collider (LHeC), where it is a high-energy lepton-proton and lepton-nucleus collider based at CERN [2]. The kinematic range in the (x, Q^2) plane of the LHeC for electron and positron neutral-current (NC) for the high energy $E_p = 7 \text{ TeV}$ is $5 \times 10^{-6} \leq x \leq 0.8$ and $5 \leq Q^2 \leq 10^6 \text{ GeV}^2$ and $5 \leq Q^2 \leq 5 \times 10^5 \text{ GeV}^2$ respectively. Today, an integrated Future Circular Collider programme consisting of a luminosity-frontier highest-energy lepton collider followed by an energy-frontier hadron collider is called FCC [3]. In this collider the FCC-eh with 50 TeV proton beams colliding with 60 GeV electrons from an energy-recovery linac would generate $\sim 2 \text{ ab}^{-1}$ of 3.5 TeV ep collisions. Deep

inelastic scattering measurements at FCC-eh will allow the determination of the gluon saturation phenomena required to unitarise the high-energy cross sections. The determination of the high gluon densities and non-linear dynamics at very small x is relevant to the interactions of cosmic ultra high energy neutrinos. For HERA data, the gluon density is not determined at low x . But, with the FCC-eh, a precision of a few percent at small x becomes possible down to nearly $x \simeq 10^{-6}$ [3].

The gluon and quark distributions are determined mainly by the proton structure function $F_2^{\gamma p}(x, Q^2)$ measured in ep DIS. The longitudinal structure function and the slope of the transverse structure function become direct probes of the gluon and sea quark distributions, over a large domain of values of x and Q^2 (hereafter Q^2 is the virtuality of the photon). Due to its origin, F_L is directly sensitive to the gluon distribution in the proton and consequently it is an important quantity [4]. In perturbative quantum chromodynamics (pQCD) the heavy quark production at HERA proceeds is dominantly via the direct BGF. Therefore, once the distribution of the gluon inside the proton is known, the heavy quark distribution can be easily calculated from it. This process can be created when the squared invariant mass of the hadronic final state has the condition the runs as follows $W^2 \geq 4m_{\text{Heavy-quark}}^2$. At very low x , the parton density cannot grow forever because hadronic cross-sections comply with the unitary bound known as Froissart Bound [5]. For this region the gluon recombination is known to provide the mechanism responsible for the unitarization of the cross section at high energies. In other words, the multiple gluon-gluon interactions provide nonlinear corrections in the DGLAP evolution equations [6]. While the precise measurement of F_L at the FCC-eh and F_2 can discover whether gluon

*brezaei@razi.ac.ir

†Electronic address: grboroun@gmail.com; boroun@razi.ac.ir

saturates.

We know that the DGLAP evolution equations are the basic perturbative tools to study the Q^2 evolution of parton distribution functions (PDFs) in the deep inelastic regime. The solutions of the coupled DGLAP evolution equations will provide the gluon and singlet quark distributions inside the nucleon at small x . These distribution functions have been determined simultaneously by starting with a virtuality $Q_0^2 \leq (m_c^2 \approx 2 \text{ GeV}^2)$ [7]. The initial distributions for the parton distributions usually are determined in a global QCD analysis including a wide range of DIS data from collider until fixed experiments. In Ref.[8], a new form of the DIS structure function (SF) $F_2(x, Q^2)$ in the domain $10^{-3} \leq x \leq 0.09$ and $0.11 \text{ GeV}^2 \leq Q^2 \leq 1200 \text{ GeV}^2$ of HERA data was proposed. This new form of the proton structure function leads to the small x asymptotics of the reduced cross-sections $\sim \ln^2 1/x$, which is in turn in an agreement with the Froissard predictions [5]. The modified form of the proton structure function with a new parametrization which describes fairly well the available experimental data, at asymptotically small x , have been presented in Refs.[9-10]. This parametrization suggested is pertinent in investigations of lepton-hadron processes at ultra-high energies, which obtained from a combined fit of the H1 and ZEUS collaborations data [11] in a range of the kinematical variables x and Q^2 , $x \leq 0.1$ and $0.15 \text{ GeV}^2 \leq Q^2 \leq 3000 \text{ GeV}^2$.

In Ref.[12], an analytical relation has been derived for calculating the gluon distribution function within the Laplace-transform method at leading order. The gluon distribution is determined by the parametrization of F_2 (Ref.[8]) as a simultaneous function of x and Q^2 in a domain $x_{min} \leq x \leq x_{max}$ and $Q_{min}^2 \leq Q^2 \leq Q_{max}^2$. Then, in Ref.[13], authors extended those previous derivation of the gluon distribution at leading order to include the effects of heavy-quark mass. These analytical solutions of the gluon behavior using a differential-equation method [12] and a Laplace transform technique [13] have been reported with considerable phenomenological success at leading order (LO) approximation respectively. Also the solutions of the unpolarized DGLAP equation for the QCD evolution of gluon distribution have been discussed considerably over the past years [14,15]. In two recent papers [16-17] the behavior of the gluon distribution function $G(x, Q^2)$ studied at small values of x by using a global parameterization of the data on $F_2(x, Q^2)$ at LO analysis.

In the present paper we study the behavior of the gluon distribution function using the proton structure function and its derivatives with respect to $\ln Q^2$ in high-order corrections based on the hard-pomeron exchange [4,18]. Then we estimate the nonlinear corrections to the gluon distribution function behavior at small values of x . Therefore, to obtain a precise evidence of the nonlinear corrections in the HERA kinematic region, we consider

the longitudinal structure function that directly depends on the behavior of the gluon distribution in which the active quarks are treated as massless. Then we generalize to the case of reduced cross section using the same method. We use the modified nonlinear corrections and higher twist predictions in obtaining our analytical solutions at low Q^2 and low x . A completed comparison between the obtained results at NNLO approximation and available DIS data are presented.

Analytical treatment of the gluon distribution function

The DGLAP evolution equation for the singlet quark structure function is given by

$$\frac{\partial F_2^s(x, Q^2)}{\partial \ln Q^2} = \frac{\alpha_s}{2\pi} \int_x^1 dz [P_{qq}(z, \alpha_s(Q^2)) F_2^s\left(\frac{x}{z}, Q^2\right) + 2N_f P_{qg}(z, \alpha_s(Q^2)) G\left(\frac{x}{z}, Q^2\right)] \quad (1)$$

where $F_2^s(x, Q^2)$ and $G(x, Q^2)$ are singlet and gluon distribution functions. Here the representation for the gluon distribution $G(x, Q^2) = xg(x, Q^2)$ is used where $g(x, Q^2)$ is the gluon density. The splitting functions $P_{ij,s}$ are the LO, NLO and NNLO Altarelli- Parisi splitting kernels as

$$P_{ij}(x, \alpha_s(Q^2)) = P_{ij}^{\text{LO}}(x) + \frac{\alpha_s(Q^2)}{2\pi} P_{ij}^{\text{NLO}}(x) + \left(\frac{\alpha_s(Q^2)}{2\pi}\right)^2 P_{ij}^{\text{NNLO}}(x), \quad (2)$$

which the explicit forms of the splitting functions at LO upto NNLO are given in Appendix A.

The running coupling constant α_s has the following forms in LO, NLO and NNLO approximation respectively [21]

$$\alpha_s^{\text{LO}} = \frac{4\pi}{\beta_0 t}, \quad (3)$$

$$\alpha_s^{\text{NLO}} = \frac{4\pi}{\beta_0 t} \left[1 - \frac{\beta_1 \ln t}{\beta_0^2 t} \right], \quad (4)$$

and

$$\alpha_s^{\text{NNLO}} = \frac{4\pi}{\beta_0 t} \left[1 - \frac{\beta_1 \ln t}{\beta_0^2 t} + \frac{1}{(\beta_0 t)^2} \left[\left(\frac{\beta_1}{\beta_0} \right)^2 (\ln^2 t - \ln t + 1) + \frac{\beta_2}{\beta_0} \right] \right]. \quad (5)$$

where $\beta_0 = \frac{1}{3}(33 - 2n_f)$, $\beta_1 = 102 - \frac{38}{3}n_f$ and $\beta_2 = \frac{2857}{6} - \frac{6673}{18}n_f + \frac{325}{54}n_f^2$. The variable t is defined as $t = \ln(\frac{Q^2}{\Lambda^2})$ and Λ is the QCD cut-off parameter at each heavy quark mass threshold as we take the $n_f = 4$ for $m_c^2 < \mu^2 < m_b^2$.

The power law behavior of the singlet and gluon distribution functions introduced as $F_2^s \sim x^{-\lambda_s}$ and $G \sim x^{-\lambda_g}$ [4,18] where exponents λ_s and λ_g are given as the derivatives: $\lambda_s = \frac{\partial \ln F_2^s(x, Q^2)}{\partial \ln(1/x)}$ and $\lambda_g = \frac{\partial \ln G(x, Q^2)}{\partial \ln(1/x)}$. By considering the hard-power behavior of the singlet and gluon distribution functions, one can rewrite the evolution equation in terms of the convolution integrals, using the convolution symbol \otimes , as

$$\begin{aligned} \frac{\partial F_2(x, Q^2)}{\partial \ln Q^2} &= F_2(x, Q^2) \Phi_{qq}(x, Q^2) \\ &+ G(x, Q^2) \Theta_{gg}(x, Q^2), \end{aligned} \quad (6)$$

where $F_2 = \frac{5}{18} F_2^s$ and the nonsinglet contribution is negligible at small x and can be ignored. The kernels for the quark and gluon sectors, denoted by Φ and Θ , presented at LO up to NNLO respectively as

$$\begin{aligned} \Theta_{gg}(x, Q^2) &= P_{gg}(x, \alpha_s) \odot x^{\lambda_g}, \\ \Phi_{qq}(x, Q^2) &= P_{qq}(x, \alpha_s) \odot x^{\lambda_s}, \end{aligned} \quad (7)$$

where $f(x) \odot g(x) \equiv \int_x^1 (dy/y) f(y) g(y)$. The splitting functions expanded into one, two and three loops cor-

rection in accordance with Appendix A.

The singlet exponent λ_s is found to be $\simeq 0.33$ in Refs.[22-23] and the gluon exponent λ_g is found to be $\simeq 0.43$ [4,18,23]. Therefore the gluon distribution function is defined by the following form

$$G(x, Q^2) = \frac{1}{\Theta_{gg}(x, Q^2)} \left[\frac{\partial F_2(x, Q^2)}{\partial \ln Q^2} - \Phi_{qq}(x, Q^2) F_2(x, Q^2) \right], \quad (8)$$

where the parameterization $F_2(x, Q^2)$ and its derivatives suggested in Refs.[8-10]. This result is general and simple and gives the leading order upto high-order expressions for the gluon distribution once the parameterization F_2 is known (Appendix B). This relation primarily comes from the extension of range and precision in the measurements of $F_2(x, Q^2)$ and $\frac{\partial F_2(x, Q^2)}{\partial \ln Q^2}$, which at small x are measures of the gluon density.

We write our final analytical answer by the following form as

$$G(x, Q^2) = \frac{1}{\{P_{gg}(x, \alpha_s) \odot x^{\lambda_g}\}} \left[\frac{\partial F_2(x, Q^2)}{\partial \ln Q^2} - \{P_{qq}(x, \alpha_s) \odot x^{\lambda_s}\} F_2(x, Q^2) \right]. \quad (9)$$

By using the leading-order splitting functions presented in Appendix A, the gluon distribution function will arrive

at

$$\begin{aligned} G^{\text{LO}}(x, Q^2) &= \frac{\frac{9\pi}{5\alpha_s}}{\int_x^1 (z^2 + (1-z)^2) z^{\lambda_g} dz} \left[\frac{\partial F_2(x, Q^2)}{\partial \ln Q^2} - \left(\frac{\alpha_s}{4\pi} \left\{ 4 + \frac{16}{3} \ln\left(\frac{1-x}{x}\right) + \frac{16}{3} \int_x^1 \frac{z^{\lambda_s} - z^{-1}}{1-z} dz \right. \right. \right. \\ &\quad \left. \left. \left. - \frac{8}{3} \int_x^1 (1+z) z^{\lambda_s} dz \right\} \right) F_2(x, Q^2) \right]. \end{aligned} \quad (10)$$

The relations in Eqs.(8) until (10) give the leading order and high-order expression for gluon distribution function in terms of a function determined by the proton structure function.

Further consideration

We now discuss how the presented results give the independent evolution equation for the singlet structure

function at small x . The DGLAP evolution equation for the gluon distribution is given by

$$\begin{aligned} \frac{\partial G(x, Q^2)}{\partial \ln Q^2} &= G(x, Q^2) \Phi_{gg}(x, Q^2) \\ &+ F_2(x, Q^2) \Theta_{gg}(x, Q^2), \end{aligned} \quad (11)$$

where kernels are

$$\begin{aligned}\Theta_{gq}(x, Q^2) &= P_{gq}(x, \alpha_s) \odot x^{\lambda_s}, \\ \Phi_{gg}(x, Q^2) &= P_{gg}(x, \alpha_s) \odot x^{\lambda_g}.\end{aligned}\quad (12)$$

Let us consider the evolution of the gluon distribution $G(x, Q^2)$ (Eq.8) with respect to $\ln Q^2$:

For fixed coupling case

After some rearranging a homogeneous second-order differential equation is found. It is determined the proton structure function $F_2(x, Q^2)$ without having knowledge in terms of the gluon distribution function, as

$$\frac{\partial^2 F_2(x, Q^2)}{\partial \ln^2 Q^2} - [\Phi_{qq}(x, Q^2) + \Phi_{gg}(x, Q^2)] \frac{\partial F_2(x, Q^2)}{\partial \ln Q^2} + [\Phi_{qq}(x, Q^2)\Phi_{gg}(x, Q^2) - \Theta_{qg}(x, Q^2)\Theta_{gq}(x, Q^2)]F_2(x, Q^2) = 0 \quad (14)$$

For running coupling case

The evolution of the gluon distribution $G(x, Q^2)$ (Eq.8) with respect to $\ln Q^2$ is given by

$$\begin{aligned}\frac{\partial G(x, Q^2)}{\partial \ln Q^2} &= \frac{\partial}{\partial \ln Q^2} \left(\frac{1}{\Theta_{qg}(x, Q^2)} \right) \left[\frac{\partial F_2(x, Q^2)}{\partial \ln Q^2} - \Phi_{qq}(x, Q^2)F_2(x, Q^2) \right] + \frac{1}{\Theta_{qg}(x, Q^2)} \left[\frac{\partial^2 F_2(x, Q^2)}{\partial \ln^2 Q^2} \right. \\ &\quad \left. - \frac{\partial \Phi_{qq}(x, Q^2)}{\partial \ln Q^2} F_2(x, Q^2) - \Phi_{qq}(x, Q^2) \frac{\partial F_2(x, Q^2)}{\partial \ln Q^2} \right].\end{aligned}\quad (15)$$

In this case the evolution equation for the singlet struc-

ture function decoupled takes the form

$$\begin{aligned}\frac{\partial^2 F_2(x, Q^2)}{\partial \ln^2 Q^2} - \left[\frac{\partial \ln \Theta_{qg}(x, Q^2)}{\partial \ln Q^2} + \Phi_{qq}(x, Q^2) + \Phi_{gg}(x, Q^2) \right] \frac{\partial F_2(x, Q^2)}{\partial \ln Q^2} \\ + [\Phi_{qq}(x, Q^2) \frac{\partial \ln \Theta_{qg}(x, Q^2)}{\partial \ln Q^2} - \frac{\partial \Phi_{qq}(x, Q^2)}{\partial \ln Q^2} + \Phi_{qq}(x, Q^2)\Phi_{gg}(x, Q^2) - \Theta_{qg}(x, Q^2)\Theta_{gq}(x, Q^2)]F_2(x, Q^2) = 0\end{aligned}\quad (16)$$

Solution for $\sigma_r(x, Q^2)$ using a Froissart bounded structure function $F_2(x, Q^2)$

The reduced neutral current (NC) deep inelastic ep scattering cross sections are given by a linear combination of generalised structure functions. The proton structure functions F_2 and F_L are related to the γ^*p cross sections of longitudinally and transversely polarized photons σ_L and σ_T as $F_L \propto \sigma_L$ and $F_T \propto \sigma_L + \sigma_T$. In one photon exchange approximation, at low and moderate

Q^2 (i.e., $Q^2 \leq M_z^2 \approx 800 \text{ GeV}^2$), the reduced cross section is defined into the transverse and longitudinal structure functions, $F_2(x, Q^2)$ and $F_L(x, Q^2)$, by the following form

$$\sigma_r(x, Q^2) = F_2(x, Q^2) - \frac{y^2}{Y_+} F_L(x, Q^2). \quad (17)$$

Here $Y_+ = 1 + (1 - y)^2$, $y = Q^2/xs$ is the inelasticity and s is the center-of-mass squared energy of incoming electrons and protons. The contribution of the term containing the longitudinal structure function F_L is only

significant for values of y larger than approximately 0.5. Indeed, the longitudinal structure function is predominant in the cross section in case of scattering of cosmic neutrinos from hadrons [27,14]. Thus, the longitudinal structure function at low x will be checked in high energy process such as the Large Hadron electron Collider (LHeC) project which runs to beyond a TeV in center-of-mass energy [1].

In perturbative QCD, the longitudinal structure function in terms of the coefficient functions is given by [28]

$$x^{-1}F_L = C_{L,ns} \otimes q_{ns} + \langle e^2 \rangle (C_{L,q} \otimes q_s + C_{L,g} \otimes g), \quad (18)$$

where the non-singlet quark distribution, xq_{ns} , become negligibly small in comparison with the singlet and gluon distribution functions, xq_n and xg , at low values of x and can be ignored. $\langle e^k \rangle$ is the average of the charge e^k for the active quark flavors, $\langle e^k \rangle = n_f^{-1} \sum_{i=1}^{n_f} e_i^k$. The average squared charge for even n_f is equal to 5/18. The symbol \otimes denotes a convolution according to the usual prescription, $f(x) \otimes g(x) = \int_x^1 \frac{dy}{y} f(y) g(\frac{x}{y})$. The perturbative expansion of the coefficient functions can be writ-

ten as [29]

$$C_{L,a}(\alpha_s, x) = \sum_{n=1} a(t)^n c_{L,a}^n(x), \quad (19)$$

where n is the order in the running coupling constant. The running coupling constant in the high-loop corrections of the above equation is expressed entirely thorough the variable $a(t)$, as $a(t) = \frac{\alpha_s}{4\pi}$. The explicit expression for the coefficient functions in LO upto NNLO are relegated in Appendix C.

Exploiting the small- x behavior of the distribution functions according to the hard (Lipatov) Pomeron, then Eq.(18) can be written as

$$F_L(x, Q^2) = F_2(x, Q^2) I_{L,s}(x, Q^2) + G(x, Q^2) I_{L,g}(x, Q^2), \quad (20)$$

where $I_{L,s}(x, Q^2) = C_{L,q}(\alpha_s, x) \odot x^{\lambda_s}$ and $I_{L,g}(x, Q^2) = \langle e^2 \rangle C_{L,g}(\alpha_s, x) \odot x^{\lambda_g}$. On this basis the reduced cross section obtain by employing the parametrization of $F_2(x, Q^2)$ as

$$\begin{aligned} \sigma_r(x, Q^2) &= F_2(x, Q^2) \left\{ 1 - \frac{y^2}{Y_+} I_{L,s}(x, Q^2) \right\} - \frac{y^2}{Y_+} I_{L,g}(x, Q^2) G(x, Q^2) [\equiv Eq.8] \\ &= F_2(x, Q^2) \left\{ 1 - \frac{y^2}{Y_+} (I_{L,s}(x, Q^2) - \frac{\Phi_{qq}(x, Q^2)}{\Theta_{qg}(x, Q^2)} I_{L,g}(x, Q^2)) \right\} - \frac{\partial F_2(x, Q^2)}{\partial \ln Q^2} \left\{ \frac{y^2}{Y_+} \frac{I_{L,g}(x, Q^2)}{\Theta_{qg}(x, Q^2)} \right\}. \end{aligned} \quad (21)$$

Therefore an explicit equation for reduced cross section in terms of the proton structure function parametrization and its derivatives is obtained.

Nonlinear and Higher Twist corrections

Nonlinear corrections:

The screening effects are provided by a multiple gluon interaction which leads to the nonlinear terms in the derivation of the linear DGLAP evolution equations. Therefore the standard linear DGLAP evolution equations will have to be modified in order to take the nonlinear corrections into account. Indeed the origin of the shadowing correction, in pQCD interactions, is primarily considered as the gluon recombination ($g + g \rightarrow g$) which is simply the inverse process of gluon splitting ($g \rightarrow g + g$). Gribov, Levin, Ryskin, Mueller and Qiu (GLR-MQ) [30] performed a detailed study of these recombination processes. This widely known as the GLR-MQ equation and involves the two-gluon distribution per unit area of the

hadron. This equation predicts a saturation behavior of the gluon distribution at very small x [31]. A closer examination of the small x scattering is resummation powers of $\alpha_s \ln(1/x)$ where leads to the k_T -factorization form [32]. In the k_T -factorization approach the large logarithms $\ln(1/x)$ are relevant for the unintegrated gluon density in a nonlinear equation. Solution of this equation develops a saturation scale where tame the gluon density behavior at low values of x and this is an intrinsic characteristic of a dense gluon system.

Therefore one should consider the low- x behavior of the singlet distribution using the nonlinear GLR-MQ evolution equation. The shadowing correction to the evolution of the singlet quark distribution can be written as [33]

$$\begin{aligned} \frac{\partial xq(x, Q^2)}{\partial \ln Q^2} &= \frac{\partial xq(x, Q^2)}{\partial \ln Q^2} \Big|_{DGLAP} \\ &\quad - \frac{27\alpha_s^2}{160R^2 Q^2} [xg(x, Q^2)]^2. \end{aligned} \quad (22)$$

Eq. (22) can be rewrite in a convenient form as

$$\frac{\partial F_2(x, Q^2)}{\partial \ln Q^2} = \frac{\partial F_2(x, Q^2)}{\partial \ln Q^2} \Big|_{DGLAP} - \frac{5}{18} \frac{27\alpha_s^2}{160R^2Q^2} \times [xg(x, Q^2)]^2. \quad (23)$$

The first term is the standard DGLAP evolution equation and the value of R is the correlation radius between two interacting gluons. It will be of the order of the proton radius ($R \simeq 5 \text{ GeV}^{-1}$), if the gluons are distributed through the whole of proton, or much smaller ($R \simeq 2 \text{ GeV}^{-1}$) if gluons are concentrated in hot-spot within the proton.

Also there is another mechanism to prevent generation of the high density gluon states, as this is well known the vacuum color screening [34]. There is a transition between the nonperturbative and perturbative domains. In the QCD vacuum, the non-perturbative fields form structures with sizes $\sim R_c$ which it is smaller than Λ_{QCD} . The short propagation length for perturbative gluons is $R_c \sim 0.2 - 0.3 \text{ fm}$. The gluon fusion effect in non-linear regime controlled by the new dimensionless parameter $\sim \frac{R_c^2}{8B}$ where B is the characteristic size of the interaction region as this parameter can be defined by $\ln(x_0/x)$ and r where $r^2 \sim Q^{-2}$. Authors in this reference (i.e., Ref.[34]) show that the nonlinear effects leads to the logarithmically ratio as the nonlinear/linear effects are proportional to $R_c^2/8B(\ln(x_0/x), r^2) \ln(Q^2 R_c^2)$.

Combining Eqs. (8) and (23), one could consider the nonlinear correction to the gluon distribution function as

$$G(x, Q^2) = \frac{1}{\Theta_{qg}(x, Q^2)} \left[\frac{\partial F_2(x, Q^2)}{\partial \ln Q^2} - \frac{5}{18} \frac{27\alpha_s^2}{160R^2Q^2} \times G^2(x, Q^2) - \Phi_{qg}(x, Q^2) F_2(x, Q^2) \right], \quad (24)$$

where

$$G(x, Q^2) + \frac{1}{\Theta_{qg}(x, Q^2)} \frac{5}{18} \frac{27\alpha_s^2}{160R^2Q^2} G^2(x, Q^2) = \frac{1}{\Theta_{qg}(x, Q^2)} \left[\frac{\partial F_2(x, Q^2)}{\partial \ln Q^2} - \Phi_{qg}(x, Q^2) F_2(x, Q^2) \right]. \quad (25)$$

Eq.(25) is a second-order equation which can be solved as

$$\begin{aligned} G(x, Q^2) &= \mathcal{F}(x, Q^2) \left[1 - \frac{\mathcal{A}(x, Q^2)}{\Theta_{qg}(x, Q^2)} \mathcal{F}(x, Q^2) \right. \\ &\quad + 2 \left(\frac{\mathcal{A}(x, Q^2)}{\Theta_{qg}(x, Q^2)} \mathcal{F}(x, Q^2) \right)^2 \\ &\quad \left. - 5 \left(\frac{\mathcal{A}(x, Q^2)}{\Theta_{qg}(x, Q^2)} \mathcal{F}(x, Q^2) \right)^3 + \dots \right] \\ &= \mathcal{F}(x, Q^2) [1 - \mathcal{N} + 2\mathcal{N}^2 - 5\mathcal{N}^3 + \dots] \\ &= \mathcal{F}(x, Q^2) [\mathcal{N}\mathcal{L}\mathcal{C}], \end{aligned} \quad (26)$$

where $\mathcal{N}\mathcal{L}\mathcal{C} = \frac{\mathcal{A}(x, Q^2)}{\Theta_{qg}(x, Q^2)} \mathcal{F}(x, Q^2)$, $\mathcal{A}(x, Q^2) = \frac{5}{18} \frac{27\alpha_s^2}{160R^2Q^2}$ and $\mathcal{F}(x, Q^2) = \frac{1}{\Theta_{qg}(x, Q^2)} \left[\frac{\partial F_2(x, Q^2)}{\partial \ln Q^2} - \Phi_{qg}(x, Q^2) F_2(x, Q^2) \right]$. Therefore the nonlinear corrections ($\mathcal{N}\mathcal{L}\mathcal{C}s$) to the reduced cross section are obtained by the following forms

$$\sigma_r(x, Q^2)|_{NLC} = F_2(x, Q^2) \left\{ 1 - \frac{y^2}{Y_+} (I_{L,s}(x, Q^2) - \frac{\Phi_{qg}(x, Q^2)}{\Theta_{qg}(x, Q^2)} I_{L,g}(x, Q^2) [\mathcal{N}\mathcal{L}\mathcal{C}]) \right\} - \frac{\partial F_2(x, Q^2)}{\partial \ln Q^2} \left\{ \frac{y^2}{Y_+} \frac{I_{L,g}(x, Q^2)}{\Theta_{qg}(x, Q^2)} \right\} [\mathcal{N}\mathcal{L}\mathcal{C}]. \quad (27)$$

Higher Twist corrections:

Introduction of higher-twist terms is one possible way to extend the DGLAP framework to low Q^2 values. Such terms have been introduced at low- x values since, for the kinematics of HERA, low Q^2 is only accessed at low x . To better illustrate our calculations at low Q^2 , we added a higher twist term in the description of the structure functions for HERA data on deep inelastic scattering at low x and low Q^2 values. It can be clearly seen that our predic-

tions with respect to the higher twist (HT) analyses are comparable with data at this region. The leading twist perturbative QCD predictions of the structure function

F_2 augment by a simple higher twist term such that

$$\begin{aligned} F_2^{HT} &= F_2^{DGLAP} \left(1 + \frac{A_2}{Q^2}\right), \\ \frac{\partial F_2^{HT}(x, Q^2)}{\partial \ln Q^2} &= \frac{\partial F_2^{DGLAP}(x, Q^2)}{\partial \ln Q^2} \left(1 + \frac{A_2}{Q^2}\right) \\ &\quad - F_2^{DGLAP} \frac{A_2}{Q^2}. \end{aligned} \quad (28)$$

where $A_2^{HT} = 0.12 \pm 0.07 \text{ GeV}^2$ is a free parameter at NNLO [35-36]. Using the HT terms in Eq.(28), we can evaluate the HT corrections to the reduced cross section as

$$\begin{aligned} \sigma_r(x, Q^2)|_{HT} &= F_2(x, Q^2) \left(1 + \frac{A_2}{Q^2}\right) \left\{1 - \frac{y^2}{Y_+} \left(I_{L,s}(x, Q^2) - \frac{\Phi_{qq}(x, Q^2)}{\Theta_{qg}(x, Q^2)} I_{L,g}(x, Q^2)\right)\right\} \\ &\quad - \left[\frac{\partial F_2(x, Q^2)}{\partial \ln Q^2} \left(1 + \frac{A_2}{Q^2}\right) - F_2(x, Q^2) \frac{A_2}{Q^2}\right] \left\{\frac{y^2}{Y_+} \frac{I_{L,g}(x, Q^2)}{\Theta_{qg}(x, Q^2)}\right\}. \end{aligned} \quad (29)$$

Modified Nonlinear (MNL) and Higher Twist (HT) corrections:

To proceed further, we use the higher twist corrections

to the nonlinear behavior and put them in nonlinear corrections as a modified nonlinear correction ($\mathcal{MNL}\mathcal{C}$) propose to replace the \mathcal{NLC} as $\mathcal{MNL}\mathcal{C} \equiv \mathcal{NLC} + HTC$. The modified NLC reads

$$\mathcal{MNL}\mathcal{C} = \frac{\mathcal{A}(x, Q^2)}{\Theta_{qg}^2(x, Q^2)} \left[\left\{ \frac{\partial F_2(x, Q^2)}{\partial \ln Q^2} \left(1 + \frac{A_2}{Q^2}\right) - F_2(x, Q^2) \frac{A_2}{Q^2} \right\} - \Phi_{qq}(x, Q^2) \left\{ F_2(x, Q^2) \left(1 + \frac{A_2}{Q^2}\right) \right\} \right].$$

Following the same procedure, the modified nonlinear and higher twist corrections to the reduced cross section

can be estimated as

$$\begin{aligned} \sigma_r(x, Q^2)|_{MNL\mathcal{C}} &= F_2(x, Q^2) \left(1 + \frac{A_2}{Q^2}\right) \left\{1 - \frac{y^2}{Y_+} \left(I_{L,s}(x, Q^2) - \frac{\Phi_{qq}(x, Q^2)}{\Theta_{qg}(x, Q^2)} I_{L,g}(x, Q^2)\right) \mathcal{MNL}\mathcal{C}\right\} \\ &\quad - \left[\frac{\partial F_2(x, Q^2)}{\partial \ln Q^2} \left(1 + \frac{A_2}{Q^2}\right) - F_2(x, Q^2) \frac{A_2}{Q^2}\right] \left\{\frac{y^2}{Y_+} \frac{I_{L,g}(x, Q^2)}{\Theta_{qg}(x, Q^2)}\right\} \mathcal{MNL}\mathcal{C}. \end{aligned} \quad (30)$$

Therefore we observe that our analysis is based on the gluon and reduced cross section where the structure function and its derivatives are supposed to be known and determined from the existing experimental data.

Results and Discussion

In this section, we shall present our results that have been obtained for the gluon distribution function $G(x, Q^2)$ and reduced cross section $\sigma_r(x, Q^2)$ using the hard-pomeron behavior of the parton distributions. To investigate this, a general relation (i.e., Eq.(8)) between the gluon density and proton structure function

and also the logarithmic slopes F_2 obtained. Several methods of relating the F_2 scaling violation to the gluon density at low x have been suggested previously [37-39]. Recently a similar connection between the gluon density and $\partial F_2/\partial \ln Q^2$ in FCC-eh [3] from the extension of range and precision in the measurement is suggested. Eq.(8) shows that the gluon density directly is related to F_2 and $\partial F_2/\partial \ln Q^2$. Figure 1 shows the coefficient $\frac{\Phi_{qq}}{\Theta_{qq}}$ as a function of Q^2 for the two x values 1×10^{-6} and 1×10^{-3} . The coefficient of F_2 is zero at NNLO only at $Q^2 \simeq 200 \text{ GeV}^2$ and $Q^2 \simeq 30 \text{ GeV}^2$ at low (1×10^{-6}) and moderate (1×10^{-3}) x values respectively. In what follows it is convenient to directly use the gluon distribution behavior with respect to F_2 and $\partial F_2/\partial \ln Q^2$. One can see that proton structure function and its derivative are supposed to be known with respect to the parametrizations represented in Refs.[8-10]. These parameterization obtained from a combined fit of the H1 and ZEUS collaborations data [11] in a range of the kinematical variables $x < 0.01$ and $0.15 \text{ GeV}^2 < Q^2 < 3000 \text{ GeV}^2$.

In Fig.2 the determined gluon distribution function is shown in a wide range of Q^2 values for $x = 1 \times 10^{-3}$ at LO upto NNLO approximation. The leading order gluon distribution is compared with the most parametrizations suggested at LO in Refs.[12-13]. The explicit forms of the gluon distributions are given in Appendix D. These results are accompanied with errors due to fit parametrizations of F_2 , as listed in Appendix B. In Ref.[23], the effective exponents for singlet and gluon densities have been derived which they are closer to those defined by the color dipole model and hard-pomeron exponents [40]. Here the values of λ_s and λ_g have been considered to be $\simeq 0.33$ and $\simeq 0.43$ within the range of Q^2 under study respectively. The coupling defined via the $n_f = 4$ definition of Λ_{QCD} for the ZEUS data [11] and the MRST set of partons [26]. The values of Λ_{QCD} at LO upto NNLO are displayed in Table III respectively. The predictions for the gluon distribution function in the kinematic range where it has been determined by M.M.Block collaboration [8-10, 12-13] computed and compared at low values of x .

In Ref. [10] a new parametrization of the SF $F_2(x, Q^2)$ which describes fairly well the available experimental data on the reduced cross sections have been suggested. With respect to this new parameterization, we consider the gluon behavior in a wide range of Q^2 values at low x in Fig.3. In this figure we have compared our results at LO upto NNLO approximation with those obtained by authors in Refs.[12-13] at LO approximation.

A detailed comparison has also been shown with the NNLO results from Block 2014 parameterization [10] and depicted in figure 4. In this figure our result based on the hard pomeron behavior have been presented for gluon distribution at low and moderate Q^2 values

($Q^2 = 3.5, 5, 8.5, 12$ and 20 GeV^2). These results have been compared with the NNLO analysis of JR09 model [41] and clearly show significant agreement over a wide range of x and Q^2 values.

The nonlinear corrections (NLCs) to the gluon density are considered in a wide range of Q^2 values for different values of x , viz. 1×10^{-3} , 1×10^{-5} and 1×10^{-7} respectively. In Fig.5, the effect of nonlinearity in our results is investigated for $R = 2 \text{ GeV}^{-1}$ at NNLO approximation. One can see that obtained nonlinear corrections for gluon distribution function are larger for very low x values ($x < 10^{-3}$) at low Q^2 values ($1 < Q^2 < 10 \text{ GeV}^2$) then another domains. Fig.6 represent linear and nonlinear results of of gluon distribution function for $R = 2 \text{ GeV}^{-1}$ at NNLO that have been computed from Eqs.(8) and (26) for $Q^2 = 3.5, 8.5$ and 20 GeV^2 respectively. It would appear that the effect of nonlinearity at low x should observe for low and moderate Q^2 . The nonlinear corrections can be neglected at large values of Q^2 , so we expect that our results are consistent in the kinematic region $x \leq 0.01$ and moderate Q^2 with other results. From these figures, it is observed that the NNLO nonlinear corrections (NNLO+NLCs) show tamed behavior compared with only NNLO approximation.

In Fig.7 we display our NNLO results for σ_r with respect to the parameterization of F_2 [10] at different proton beam energies E_p (=920, 820 and 575 GeV), relevant for most H1 measurements [42-43], where the turnover at small x becomes more pronounced at smaller energies because of the larger values of y . The data are taken with positrons of energy $E_e = 27.6 \text{ GeV}$ corresponding to the center of mass energies $\sqrt{s} = 2\sqrt{E_e E_p} [\text{GeV}]$. In Fig.8 the NNLO predictions at $\sqrt{s} = 300.9 \text{ GeV}$ are compared with H1 data [42] as accompanied with total errors. These small- x predictions are fully compatible with the H1 data presented in [42]. The modified nonlinear and higher twist corrections are depicted and compared with the linear dependence in these figures. We have also performed an analysis to check the sensitivity of the modified nonlinear and higher twist corrections in reduced cross section results.

We have calculated the Q^2 -dependence, at low x , of the reduced cross section $\sigma_r(x, Q^2)$ (i.e., Eq.(30)) in the NNLO approximation. Results of calculations and comparison with data of the H1-Collaboration [42] are presented in Fig.10, where the solid line correspond to the extracted σ_r in the NNLO approximations. Calculations have been performed at fixed value of the inelasticity y , $y = 0.675$, allowing the Bjorken variable x to vary in the interval ($3 \times 10^{-5} < x < 7 \times 10^{-4}$) when Q^2 varies in the interval ($1.5 < Q^2 < 40 \text{ GeV}^2$). To illustrate better the modified nonlinear and higher twist corrections at low Q^2 values, we have plotted MNL+HT predictions to the NNLO results in Fig.10. It may lead to the better determinations of the reduced cross section specially at low Q^2 .

thanks the Department of Physics of the CERN-TH for their warm hospitality. Also authors would like to thank H.Khanpour for discussions which completed this study.

Summary and Conclusion

We presented Eqs.(8-10) for the extraction of the gluon distribution function $G(x, Q^2)$ at low x in the leading-order upto next-to-next-to-leading order from the $F_2(x, Q^2)$ and its $\ln Q^2$ derivative. Then rendered the results for the reduced cross section $\sigma_r(x, Q^2)$ in a wide range of Q^2 values. The reduced cross section behavior is considered at low x with respect to the F_2 parameterization. This method can be used in very low x at the LHeC and FCC-eh projects. Our results at NNLO are in good agreement with the experimental data at low x values in a large interval of the momentum transfer. The obtained explicit expression for the gluon distribution function and the reduced cross section are entirely determined by the effective exponents of the singlet and gluon distribution functions. We have studied the effects of adding the nonlinear GLR-MQ corrections to the NNLO linear behavior of the gluon distribution function and reduced cross section. These results are close to the data for low- Q^2 values as we have discussed the meaning of these findings from the points of view of modified nonlinear and higher twist corrections added to the structure function. Consequently, the size of the NNLO corrections to the reduced cross section becomes possible to perform the high-order corrections to the ultra-high energy processes.

Acknowledgments

The authors appreciate the Research Council of Razi University for official support of this work. G.R.Boroun

Appendix A

The LO up to NNLO splitting functions for singlet and gluon distribution functions are as follows [19-20]: At LO :

$$\begin{aligned}
 P_{qq}^{\text{LO}}(z) &= C_F \left[\frac{1+z^2}{(1-z)_+} + \frac{3}{2} \delta(1-z) \right], \\
 P_{qg}^{\text{LO}}(z) &= \frac{1}{2} (z^2 + (1-z)^2), \\
 P_{gq}^{\text{LO}}(z) &= C_F \frac{1+(1-z)^2}{z}, \\
 P_{gg}^{\text{LO}}(z) &= 2C_A \left(\frac{z}{(1-z)_+} + \frac{(1-z)}{z} + z(1-z) \right) \\
 &\quad + \delta(1-z) \frac{(11C_A - 4n_f T_R)}{6}. \tag{31}
 \end{aligned}$$

The convolution integrals which contains plus prescription, $()_+$, can be easily calculate by

$$\begin{aligned}
 \int_x^1 \frac{dy}{y} f\left(\frac{x}{y}\right)_+ g(y) &= \int_x^1 \frac{dy}{y} f\left(\frac{x}{y}\right) \left[g(y) - \frac{x}{y} g(x) \right] \\
 &\quad - g(x) \int_0^x f(y) dy \tag{32}
 \end{aligned}$$

At NLO :

$$\begin{aligned}
P_{qq}^{\text{NLO}} &= (C_F)^2(-1+z+(1/2-3/2z)\ln(z)-1/2(1+z)\ln(z)^2-(3/2\ln(z)+2\ln(z)\ln(1-z))p_{qq}(z) \\
&\quad +2p_{qq}(-z)S_2(z)) + C_F C_A(14/3(1-z)+(11/6\ln(z)+1/2\ln(z)^2+67/18-\pi^2/6)p_{qq}(z) \\
&\quad -p_{qq}(-z)S_2(z)) + C_F T_F(-16/3+40/3z+(10z+16/3z^2+2)\ln(z)-112/9z^2+40/(9z) \\
&\quad -2(1+z)\ln(z)^2-(10/9+2/3\ln(z))p_{qq}(z)). \\
P_{qg}^{\text{NLO}} &= C_F T_F(4-9z-(1-4z)\ln(z)-(1-2z)\ln(z)^2+4\ln(1-z)+(2\ln((1-z)/z)^2-4\ln((1-z)/z) \\
&\quad -2/3\pi^2+10)P_{qg}(z)) + C_A T_F(182/9+14/9z+40/(9z)+(136/3z-38/3)\ln(z)-4\ln(1-z) \\
&\quad -(2+8z)\ln(z)^2+2P_{qg}(-z)S_2(z)+(-\ln(z)^2+44/3\ln(z)-2\ln(1-z)^2+4\ln(1-z) \\
&\quad +\pi^2/3-218/9)P_{qg}(z)). \\
P_{gq}^{\text{NLO}} &= C_F^2(-5/2-7z/2+(2+7/2z)\ln(z)-(1-z/2)\ln(z)^2-2z\ln(1-z)-(3\ln(1-z) \\
&\quad +\ln(1-z)^2)P_{gq}(z)) + C_F C_A(28/9+65/18z+44/9z^2-(12+5z+8/3z^2)\ln(z)+(4+z)\ln(z)^2 \\
&\quad +2z\ln(1-z)+S_2(z)P_{gq}(-z)+(1/2-2\ln(z)\ln(1-z)+1/2\ln(z)^2+11/3\ln(1-z)+\ln(1-z)^2 \\
&\quad -\pi^2/6)P_{gq}(z)) + C_F T_F(-4/3z-(20/9+4/3\ln(1-z))P_{gq}(z)). \\
P_{gg}^{\text{NLO}} &= C_F T_F(-16+8z+20/3z^2+4/(3z)-(6+10z)\ln(z)-(2+2z)\ln(z)^2) + C_A T_F(2-2z \\
&\quad +26/9(z^2-1/z)-4/3(1+z)\ln(z)-20/9P_{gg}(z)) + C_A^2(27/2(1-z)+26/9(z^2-1/z) \\
&\quad -(25/3-11/3z+44/3z^2)\ln(z)+4(1+z)\ln(z)^2+2P_{gg}(-z)S_2(z)+(67/9-4\ln(z)\ln(1-z) \\
&\quad +\ln(z)^2-\pi^2/3)P_{gg}(z)).
\end{aligned} \tag{33}$$

where

At NNLO :

$$\begin{aligned}
p_{qq}(z) &= 2/(1-z) - 1 - z \\
p_{qq}(-z) &= 2/(1+z) - 1 + z \\
P_{qg}(z) &= z^2 + (1-z)^2 \\
P_{qg}(-z) &= z^2 + (1+z)^2 \\
P_{gq}(z) &= (1+(1-z)^2)/z \\
P_{gq}(-z) &= -(1+(1+z)^2)/z \\
P_{gg}(z) &= 1/(1-z) + 1/z - 2 + z(1-z) \\
P_{gg}(-z) &= 1/(1+z) - 1/z - 2 - z(1+z) \\
S_2(z) &= \int_{1/(1+z)}^{z/(1+z)} 1/y \ln((1-y)/y) dy
\end{aligned} \tag{34}$$

$$\begin{aligned}
P_{qq}^{\text{NNLO}} &= (n_f(-5.926L_1^3 - 9.751L_1^2 - 72.11L_1 + 177.4 + 392.9z - 101.4z^2 - 57.04L_0L_1 - 661.6L_0 \\
&\quad + 131.4L_0^2 - 400/9L_0^3 + 160/27L_0^4 - 506/z - 3584/271/zL_0) + n_f^2(1.778L_1^2 + 5.944L_1 \\
&\quad + 100.1 - 125.2z + 49.26z^2 - 12.59z^3 - 1.889L_0L_1 + 61.75L_0 + 17.89L_0^2 + 32/27L_0^3 \\
&\quad + 256/811/z))(1-z). \\
P_{qg}^{\text{NNLO}} &= n_f(100/27L_1^4 - 70/9L_1^3 - 120.5L_1^2 + 104.42L_1 + 2522 - 3316z + 2126z^2 \\
&\quad + L_0L_1(1823 - 25.22L_0) - 252.5zL_0^3 + 424.9L_0 + 881.5L_0^2 - 44/3L_0^3 + 536/27L_0^4 \\
&\quad - 1268.31/z - 896/31/zL_0) + n_f^2(20/27L_1^3 + 200/27L_1^2 - 5.496L_1 - 252 + 158z + 145.4z^2 \\
&\quad - 139.28z^3 - L_0L_1(53.09 + 80.616L_0) - 98.07zL_0^2 + 11.70zL_0^3 - 254L_0 - 98.80L_0^2 - 376/27L_0^3 \\
&\quad - 16/9L_0^4 + 1112/2431/z). \\
P_{gq}^{\text{NNLO}} &= 400/81L_1^4 + 2200/27L_1^3 + 606.3L_1^2 + 2193L_1 - 4307 + 489.3z + 1452z^2 + 146z^3 - 447.3L_0^2L_1 \\
&\quad - 972.9zL_0^2 + 4033L_0 - 1794L_0^2 + 1568/9L_0^3 - 4288/81L_0^4 + 6163.11/z + 1189.31/zL_0 \\
&\quad + n_f(-400/81L_1^3 - 68.069L_1^2 - 296.7L_1 - 183.8 + 33.35z - 277.9z^2 + 108.6zL_0^2 \\
&\quad - 49.68L_0L_1 + 174.8L_0 + 20.39L_0^2 + 704/81L_0^3 + 128/27L_0^4 - 46.411/z + 71.0821/zL_0) \\
&\quad + n_f^2(96/27L_1^2(1/z - 1 + 1/2z) + 320/27L_1(1/z - 1 + 4/5z) - 64/27(1/z - 1 - 2z)). \\
P_{gg}^{\text{NNLO}} &= 2643.524D_0 + 4425.894\delta(1-z) + 3589L_1 - 20852 + 3968z - 3363z^2 + 4848z^3 \\
&\quad + L_0L_1(7305 + 8757L_0) + 274.4L_0 - 7471L_0^2 + 72L_0^3 - 144L_0^4 + 142141/z + 2675.81/zL_0 \\
&\quad + n_f(-412.142D_0 - 528.723\delta(1-z) - 320L_1 - 350.2 + 755.7z - 713.8z^2 + 559.3z^3 \\
&\quad + L_0L_1(26.15 - 808.7L_0) + 1541L_0 + 491.3L_0^2 + 832/9L_0^3 + 512/27L_0^4 + 182.961/z \\
&\quad + 157.271/zL_0) + n_f^2(-16/9D_0 + 6.4630\delta(1-z) - 13.878 + 153.4z - 187.7z^2 + 52.75z^3 \\
&\quad - L_0L_1(115.6 - 85.25z + 63.23L_0) - 3.422L_0 + 9.680L_0^2 - 32/27L_0^3 - 680/2431/z). \tag{35}
\end{aligned}$$

where $D_0 = 1/(1-z)$.

polynomial in ν as $\widehat{F}_2^{\gamma p}(\nu, Q^2) \rightarrow C_{0f}(Q^2) + C_{1f}(Q^2)\nu + C_{2f}(Q^2)\nu^2 + \widehat{O}(\nu)$ where the coefficient functions are defined in Ref. [9].

Appendix B

The proton structure function parameterized with a global fit function [9] to the HERA combined data for $F_2^{\gamma p}(x, Q^2)$ for $0.85 < Q^2 < 3000 \text{ GeV}^2$ and $x < 0.1$, which ensures that the saturated Froissart $\ln^2(1/x)$ behavior dominates at low- x . This global fit takes the form

$$\begin{aligned}
F_2^{\gamma p}(x, Q^2) &= (1-x) \left[\frac{F_P}{1-x_P} + A(Q^2) \ln\left(\frac{x_P}{x} \frac{1-x}{1-x_P}\right) \right. \\
&\quad \left. + B(Q^2) \ln^2\left(\frac{x_P}{x} \frac{1-x}{1-x_P}\right) \right], \tag{36}
\end{aligned}$$

where

$$A(Q^2) = a_0 + a_1 \ln Q^2 + a_2 \ln^2 Q^2,$$

and

$$B(Q^2) = b_0 + b_1 \ln Q^2 + b_2 \ln^2 Q^2.$$

The fitted parameters are tabulated in Table I. At low x (or large $\nu = \ln(1/x)$), the global fit becomes a quadratic

TABLE I: Parameters of Eq. (36), resulting from a global fit to the HERA combined data.

parameters	value
a_0	$-8.471 \times 10^{-2} \pm 2.62 \times 10^{-3}$
a_1	$4.190 \times 10^{-2} \pm 1.56 \times 10^{-3}$
a_2	$-3.976 \times 10^{-3} \pm 2.13 \times 10^{-4}$
b_0	$1.292 \times 10^{-2} \pm 3.62 \times 10^{-4}$
b_1	$2.473 \times 10^{-4} \pm 2.46 \times 10^{-4}$
b_2	$1.642 \times 10^{-3} \pm 5.52 \times 10^{-5}$
F_p	0.413 ± 0.003
$\chi^2(\text{goodness of fit})$	1.17

This form for $F_2^{\gamma p}$ (i.e. Eq.(36)) describes the HERA data well, but the model does not have the properties necessary for the $\gamma^* - p$ reduced cross section to extend smoothly to $Q^2 = 0$ limit. Authors in Ref.[10] provide

good fits to the HERA data at low x and large Q^2 values. With respect to the Block-Halzen [24] fit, The explicit expression for the proton structure function in a range of the kinematical variables x and Q^2 , $x < 0.001$ and $0.15 \text{ GeV}^2 < Q^2 < 3000 \text{ GeV}^2$, is defined by the following form

$$F_2^{\gamma p}(x, Q^2) = D(Q^2)(1-x)^n[C(Q^2) + A(Q^2) \ln(\frac{1}{x} \frac{Q^2}{Q^2 + \mu^2}) + B(Q^2) \ln^2(\frac{1}{x} \frac{Q^2}{Q^2 + \mu^2})], \quad (37)$$

where

$$\begin{aligned} A(Q^2) &= a_0 + a_1 \ln(1 + \frac{Q^2}{\mu^2}) + a_2 \ln^2(1 + \frac{Q^2}{\mu^2}), \\ B(Q^2) &= b_0 + b_1 \ln(1 + \frac{Q^2}{\mu^2}) + b_2 \ln^2(1 + \frac{Q^2}{\mu^2}), \\ C(Q^2) &= c_0 + c_1 \ln(1 + \frac{Q^2}{\mu^2}), \\ D(Q^2) &= \frac{Q^2(Q^2 + \lambda M^2)}{(Q^2 + M^2)^2}. \end{aligned} \quad (38)$$

Here M is the effective mass and μ^2 is a scale factor. The additional parameters with their statistical errors are given in Table II.

TABLE II: The effective Parameters at low x for $0.15 \text{ GeV}^2 < Q^2 < 3000 \text{ GeV}^2$ provided by the following values. The fixed parameters are defined by the Block-Halzen fit to the real photon-proton cross section as $M^2 = 0.753 \pm 0.068 \text{ GeV}^2$, $\mu^2 = 2.82 \pm 0.290 \text{ GeV}^2$ and $c_0 = 0.255 \pm 0.016$ [10].

parameters	value
a_0	$8.205 \times 10^{-4} \pm 4.62 \times 10^{-4}$
a_1	$-5.148 \times 10^{-2} \pm 8.19 \times 10^{-3}$
a_2	$-4.725 \times 10^{-3} \pm 1.01 \times 10^{-3}$
b_0	$2.217 \times 10^{-3} \pm 1.42 \times 10^{-4}$
b_1	$1.244 \times 10^{-2} \pm 8.56 \times 10^{-4}$
b_2	$5.958 \times 10^{-4} \pm 2.32 \times 10^{-4}$
C_1	$1.475 \times 10^{-1} \pm 3.025 \times 10^{-2}$
n	11.49 ± 0.99
λ	2.430 ± 0.153
$\chi^2(\text{goodness of fit})$	0.95

Appendix C

The coefficient functions for F_L have the following forms [29] as:

At LO :

$$\begin{aligned} c_{L,g}^1 &= 8n_f z(1-z), \\ c_{L,q}^1 &= 4C_F z. \end{aligned} \quad (39)$$

At NLO :

$$\begin{aligned} c_{L,g}^2 &= n_f \{ (94.74 - 49.20z)z_1 L_1^2 + 864.8z_1 L_1 \\ &\quad + 1161z L_1 L_0 + 60.06z L_0^2 + 39.66z_1 L_0 \\ &\quad - 5.333(1/z - 1) \}, \\ c_{L,q}^2 &= 128/9z L_1^2 - 46.50z L_1 - 84.094L_0 L_1 - 37.338 \\ &\quad + 89.53z + 33.82z^2 + z L_0(32.90 + 18.41L_0) \\ &\quad - 128/9L_0 - 0.012\delta(z_1) + 16/27n_f(6z L_1 \\ &\quad - 12z L_0 - 25z + 6) \\ &\quad + n_f \{ (15.94 - 5.212z)z_1^2 L_1 + (0.421 + 1.520z)L_0^2 \\ &\quad + 28.09z_1 L_0 - (2.371/z - 19.27)z_1^3 \}. \end{aligned} \quad (40)$$

At NNLO :

Appendix D

$$\begin{aligned}
c_{L,g}^3 = & n_f \{ (144L_1^4 - 47024/27L_1^3 + 6319L_1^2 + 53160L_1)z_1 \\
& + 72549L_0L_1 + 88238L_0^2L_1 + (3709 - 33514z \\
& - 9533z^2)z_1 + 66773zL_0^2 - 1117L_0 + 45.37L_0^2 \\
& - 5360/27L_0^3 - (2044.70z_1 + 409.506L_0)1/z \} \\
& + n_f^2 \{ (32/3L_1^3 - 1216/9L_1^2 - 592.3L_1 \\
& + 1511zL_1)z_1 + 311.3L_0L_1 + 14.24L_0^2L_1 \\
& + (577.3 - 729z)z_1 + 30.78zL_0^3 + 366L_0 + 1000/9L_0^2 \\
& + 160/9L_0^3 + 88.50371/z z_1 \} \\
& + fl_{11}^g n_f^2 \{ (-0.0105L_1^3 + 1.550L_1^2 + 19.72zL_1 \\
& - 66.745z + 0.615z^2)z_1 + 20/27zL_0^4 + (280/81 \\
& + 2.260z)zL_0^3 - (15.40 - 2.201z)zL_0^2 + 2.260z)zL_0^3 \\
& - (71.66 - 0.121z)zL_0 \}, \\
c_{L,q}^3 = & 512/27L_1^4 - 177.40L_1^3 + 650.6L_1^2 - 2729L_1 \\
& - 2220.5 - 7884z + 4168z^2 - (844.7L_0 \\
& + 517.3L_1)L_0L_1 + (195.6L_1 - 125.3)z_1L_1^3 \\
& + 208.3zL_0^3 - 1355.7L_0 - 7456/27L_0^2 - 1280/81L_0^3 \\
& + 0.113\delta(z_1) + n_f \{ 1024/81L_1^3 - 112.35L_1^2 + 344.1L_1 \\
& + 408.4 - 9.345z - 919.3z^2 + (239.7 + 20.63L_1)z_1L_1^2 \\
& + (887.3 + 294.5L_0 - 59.14L_1)L_0L_1 - 1792/81zL_0^3 \\
& + 200.73L_0 + 64/3L_0^2 + 0.006\delta(z_1) \} + n_f^2 \{ 3zL_1^2 \\
& + (6 - 25z)L_1 - 19 + (317/6 - 12\zeta_2)z - 6zL_0L_1 \\
& + 6zLi_2(x) + 9zL_0^2 - (6 - 50z)L_0 \} 64/81 \\
& + fl_{11}^{ns} n_f \{ (107 + 321.05z - 54.62z^2)z_1 - 26.717 \\
& + 9.773L_0 + (363.8 + 68.32L_0)zL_0 \\
& - 320/81L_0^2(2 + L_0) \} z \\
& + n_f \{ (1568/27L_1^3 - 3968/9L_1^2 + 5124L_1)z_1^2 \\
& + (2184L_0 + 6059z_1)L_0L_1 - (795.6 + 1036z)z_1^2 \\
& - 143.6z_1L_0 + 2848/9L_0^2 - 1600/27L_0^3 \\
& - (885.53z_1 + 182L_0)1/z z_1 \} + n_f^2 \{ (-32/9L_1^2 \\
& + 29.52L_1)z_1^2 + (35.18L_0 + 73.06z_1)L_0L_1 \\
& - 35.24zL_0^2 - (14.16 - 69.84z)z_1^2 - 69.41z_1L_0 \\
& - 128/9L_0^2 + 40.2391/z z_1^2 \} + fl_{11}^{ps} n_f \{ (107 \\
& + 321.05z - 54.62z^2)z_1 - 26.717 + 9.773L_0 + (363.8 \\
& + 68.32L_0)zL_0 - 320/81L_0^2(2 + L_0) \} z. \quad (41)
\end{aligned}$$

In these equations we have used the abbreviations $z_1 = 1 - z$, $L_0 = \ln z$ and $L_1 = \ln z_1$. For the SU(N) gauge group, we have $C_A = N$, $C_F = (N^2 - 1)/2N$, $T_F = n_f T_R$, and $T_R = 1/2$ where C_F and C_A are the color Cassimir operators in QCD. Also the new charge factors are defined by the following form, $fl_{11}^{ns} = 3 < e >$, $fl_{11}^g = < e >^2 / < e^2 >$ and $fl_{11}^{ps} = fl_{11}^g - fl_{11}^{ns}$.

The gluon distribution is derived from the leading order DGLAP evolution equation for $F_2(x, Q^2)$ in a domain $x \leq 0.09$ and $0.11 \text{ GeV}^2 \leq Q^2 \leq 1200 \text{ GeV}^2$. Solution for $G(x, Q^2)$ using a Froissart bounded structure function $F_2(x, Q^2)$ is obtained in terms of a quadratic polynomial in $\ln(1/x)$ with quadratic polynomial coefficients in $\ln(Q^2)$ as [12]

$$\begin{aligned}
G(x, Q^2) = & -0.459 - 0.143\ln(Q^2) - 0.0155\ln^2(Q^2) \\
& + [0.231 + 0.00971\ln(Q^2) - 0.0147\ln^2(Q^2)]\ln(1/x) \\
& + [0.0836 + 0.06328\ln(Q^2) + 0.0112\ln^2(Q^2)]\ln^2(1/x) \quad (42)
\end{aligned}$$

The above method generalized to the case of massive quarks directly from $F_2(x, Q^2)$ by Laplace transforms to the DGLAP equation [13]. The gluon distribution function for $n_f = 4$ at $Q^2 = M_b^2$ with $M_b = 4.5 \text{ GeV}$ is obtained with an expression quadratic in both $\ln(1/x)$ and $\ln(Q^2)$ by the following form

$$G_4(x, Q^2) = \frac{3}{5} \mathcal{H}_3(x, Q^2) = \mathcal{H}_4(x, Q^2), \quad (43)$$

where

$$\begin{aligned}
\mathcal{H}_3(x, Q^2) = & -2.94 - 0.359\ln(Q^2) - 0.101\ln^2(Q^2) \\
& + [0.594 - 0.0792\ln(Q^2) - 0.000578\ln^2(Q^2)]\ln(1/x) \\
& + [0.168 + 0.138\ln(Q^2) + 0.0169\ln^2(Q^2)]\ln^2(1/x). \quad (44)
\end{aligned}$$

TABLE III: The QCD coupling and corresponding Λ parameter for $n_f = 4$ at LO, NLO [25] and NNLO analysis [26].

	$\alpha_s(M_Z^2)$	$\Lambda_{QCD}(MeV)$
LO	0.1166	136.8
NLO	0.1166	284
NNLO	0.1155	235

REFERENCES

1. M. Klein, Ann. Phys.**528**, 138 (2016).
2. R.A.Khalek et al., arXiv:1906.10127 [2019].
3. A. Abada et al., [FCC Collaborations], Eur.Phys.J.**C79**, 474(2019).
4. A.Donnachie and P.V.Landshoff, Phys.Lett.B **470**, 273(1999).
5. M.Froissart, Phys.Rev.**123**, 1053 (1961).
6. Yu.L.Dokshitzer, Sov.Phys.JETP **46**, 641(1977); G.Altarelli and G.Parisi, Nucl.Phys.B **126**, 298(1977); V.N.Gribov and L.N.Lipatov, Sov.J.Nucl.Phys. **15**, 438(1972).
7. H.Khanpour et al., Phys.Rev.C**95**, 035201(2017); H.Khanpour, Phys.Rev. **D99**, 054007(2019).
8. E. L. Berger, M. M. Block and C. I. Tan, Phys. Rev. Lett. **98**, 242001 (2007); M. M. Block, E. L. Berger and C. I. Tan, Phys. Rev. Lett.**97**, 252003 (2006).
9. M. M. Block, L. Durand, P. Ha and D. W. McKay, Phys. Rev.**D 84**, 094010 (2011); Phys. Rev.**D 88**, no. 1, 014006 (2013).
10. M. M. Block, L. Durand and P. Ha, Phys. Rev.**D 89**, no. 9, 094027 (2014).
11. F. D. Aaron et al. [H1 and ZEUS Collaborations], JHEP**1001**, 109 (2010).
12. M. M. Block, L. Durand and D. W. McKay, Phys. Rev.**D 77**, 094003 (2008); Phys. Rev.**D 79**, 014031 (2009).
13. M.M.Block, Eur.Phys.J.**C65**, 1(2010); M. M. Block and L. Durand, arXiv:0902.0372[hep-ph](2009).
14. K.Prytz, Phys.Lett.**B311**,286(1993); A.V.Kotikov and G.Parente, Phys.Lett.**B379**, 195(1996); G.R.Boroun and B.Rezaei, Chin.Phys.Lett.**23**, 324(2006).
15. G.R.Boroun and B.Rezaei, Eur.Phys.J.**C73**, 2412(2013); S.Zarrin and G.R.Boroun, Nucl.Phys.**B922**, 126 (2017); M.Lalung et al., Int.J.Theor.Phys.**56**, 3625(2017); M.Devee, arXiv:1808.00899(2018).
16. A.V.Kotikov, Phys.Atom.Nucl,**80**, 572 (2017).
17. N.Yu.Chernikova and A.V.Kotikov, JETP Lett.**105**, 223(2017).
18. A.Donnachie and P.V.Landshoff, Phys.Lett.B **550**, 160(2002).
19. W.L. van Neerven, A.Vogt, Phys.Lett.B **490**, 111(2000).
20. A.Vogt, S.Moch, J.A.M.Vermaseren, Nucl.Phys.B **691**, 129(2004).
21. B.G. Shaikhatdenov, A.V. Kotikov, V.G. Kri-vokhizhin, G. Parente, Phys. Rev. D **81**, 034008(2010).
22. K Golec-Biernat and A.M.Stasto, Phys.Rev.D **80**, 014006(2009); R.D.Ball et al., Eur.Phys.J. **C76**, 383(2016).
23. B.Rezaei and G.R.Boroun, Eur.Phys.J.A**55**, 66(2019); G.R.Boroun, Eur.Phys.J.A**50**, 69(2014).
24. M. M. Block and F. Halzen, Phys. Rev. **D70**, 091901(2004).
25. L.P.Kaptari et al., Phys.Rev.**D99**, 096019(2019).
26. A.D.Martin et al., Phys.Letts.**B604**, 61(2004).
27. L.A.Anchordoqui et al., arXiv:1902.10134[hep-ph].
28. G.Altarelli and G.Martinelli, Phys.Lett.**B76**, 89(1978).
29. S.Moch, J.A.M.Vermaseren and A.Vogt, Phys.Lett.**B606**, 123(2005).
30. A. H. Mueller and J. Qiu, Nucl. Phys. **B268**(1986)427; L. V. Gribov, E. M. Levin and M. G. Ryskin, Phys. Rep.**100**, (1983)1.
31. G. R. Boroun and B. Rezaei, Chin. Phys. Lett.**32**, (2015) no.11, 111101; B. Rezaei and G. R. Boroun, Phys. Lett. **B692** (2010) 247; G. R. Boroun, Eur. Phys. J. **A43** (2010) 335.
32. N. N. Nikolaev and W. Schäfer, Phys. Rev. **D74**(2006)014023.
33. K. J. Eskola et al., Nucl. Phys. **B660**(2003)211.
34. R. Fiore, P. V. Sasorov and V. R. Zoller, JETP Letters **96**(2013)687; R. Fiore, N. N. Nikolaev and V. R. Zoller, JETP Letters **99**(2014)363.
35. A.M.Cooper-Sarkar, arXiv:1605.08577v1 [hep-ph] 27 May 2016; I.Abt et.al., arXiv:1604.02299v2 [hep-ph] 11 Oct 2016.
36. F.D. Aaron et al. [H1 Collaboration], Eur.Phys.J. **C63**, 625(2009).
37. K.Prytz, Phys.Lett.**B311**, 286(1993); Phys.Lett.**B332**, 393(1994).
38. M.B.Gay Ducati and P.B.Goncalves, Phys.Lett.**B390**, 401(1997).
39. G.R.Boroun, Journal of Experimental and Theoretical Physics, **111**, 566(2010); N.N.Nikolaev and B.G.Zakharov, Phys.Lett. **B332**, 184(1994).
40. N.N.Nikolaev and B.G.Zakharov, Phys.Lett.B332, 184(1994); N.N.Nikolaev and V.R.Zoller, Phys.Atom.Nucl.**73**, 672 (2010).
41. P.Jimenez-Delgado and E.Reya, Phys.Rev.**D79**, 074023(2009).
42. C.Adloff et al., [H1 Collaboration], Eur.Phys.J.C.**21**, 33(2001).
43. F.D. Aaron et al., [H1 Collaboration], Phys.Lett.B.**665**, 139(2008).

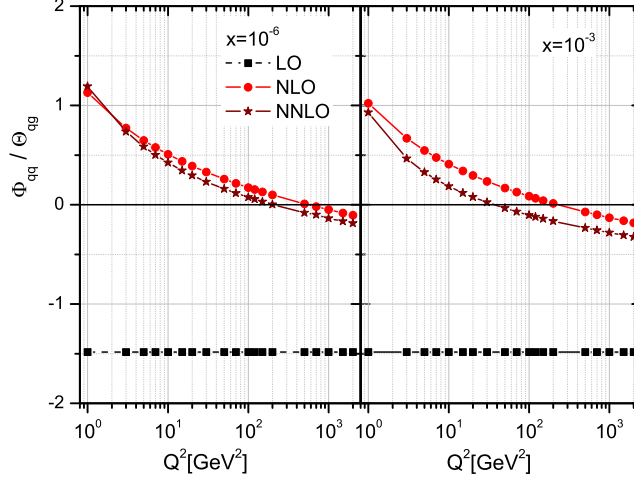


FIG. 1: Plot of the ratio $\frac{\Phi_{qq}}{\Theta_{qg}}$ as a function of Q^2 for two x (1×10^{-6} and 1×10^{-3}).

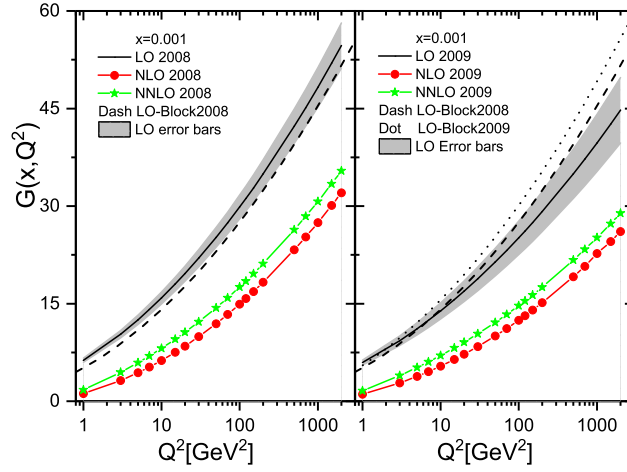


FIG. 2: The leading-order up to the next-to next-to leading order gluon distributions in comparison with the leading-order results of Block model [12-13]. The error bars are due to the F_2 parameterization at LO approximation.

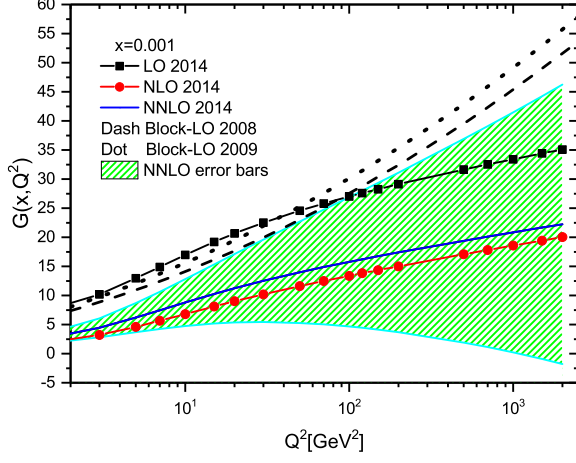


FIG. 3: The leading-order up to the next-to next-to leading order gluon distributions from the new F_2 parameterization [10] compared with the leading-order results of Block model [12-13]. The error bars are due to the F_2 parameterization at NNLO approximation.

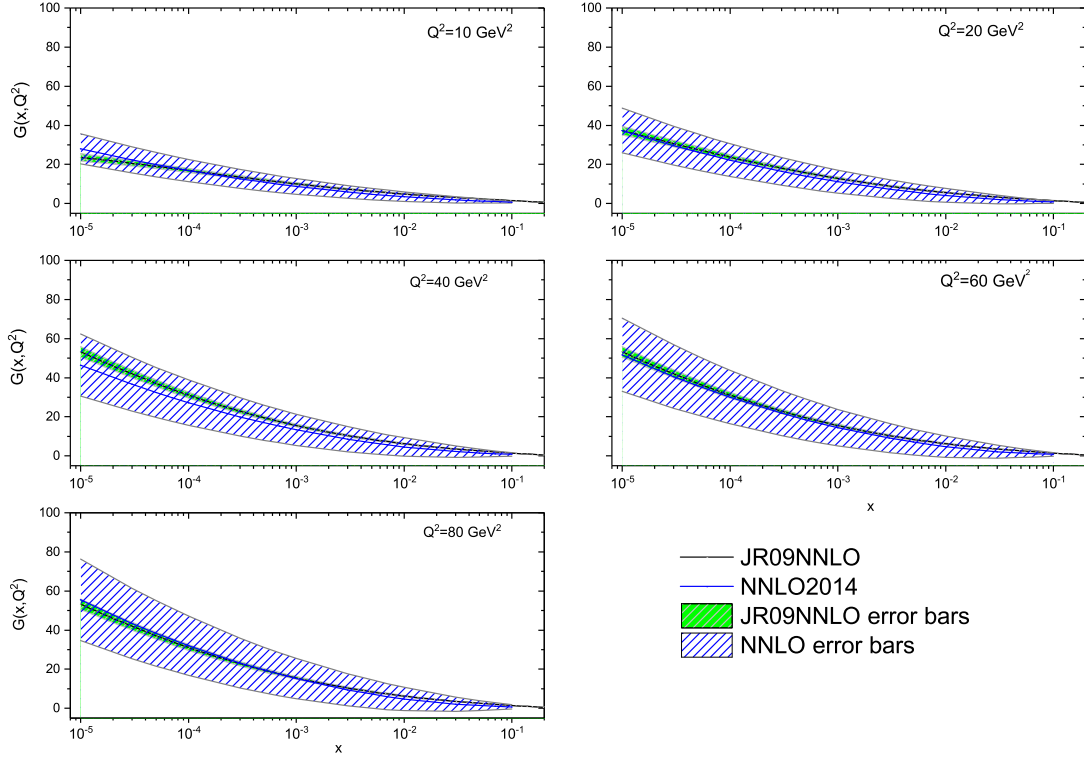


FIG. 4: The NNLO gluon distributions from the new F_2 parameterization [10] and its comparison with the results from JR09NNLO global QCD analysis [41] at $Q^2 = 10, 20, 40, 60$ and 80 GeV^2 . The error bars are due to the F_2 parameterization at NNLO approximation and JR09 NNLO analysis.

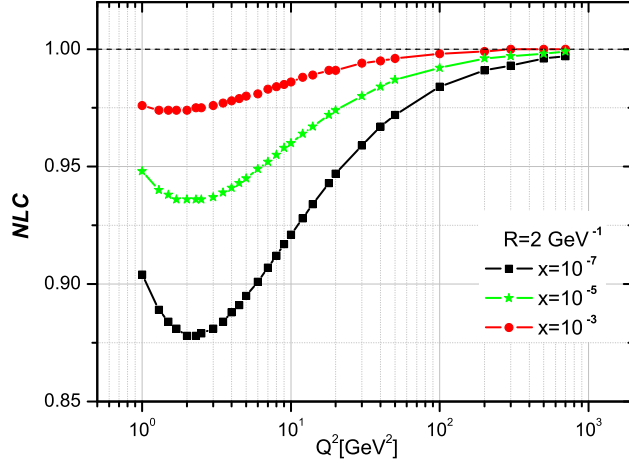


FIG. 5: Nonlinear correction (NLC) effects for $R = 2 \text{ GeV}^{-1}$ in a wide range of Q^2 at low and very low x values.

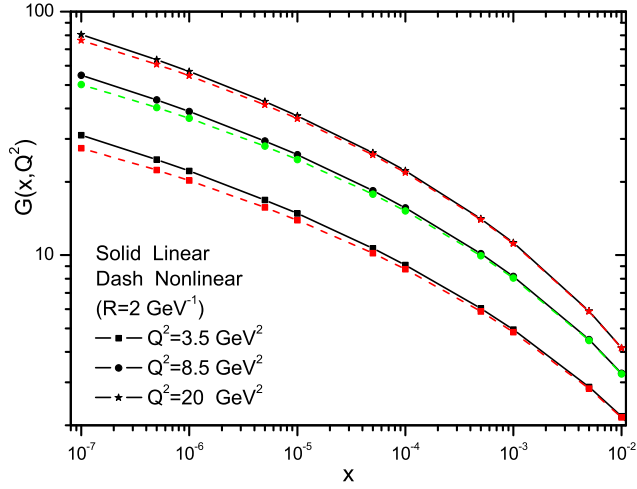


FIG. 6: x -evolution of linear and nonlinear gluon distribution function at NNLO approximation for three fixed Q^2 .

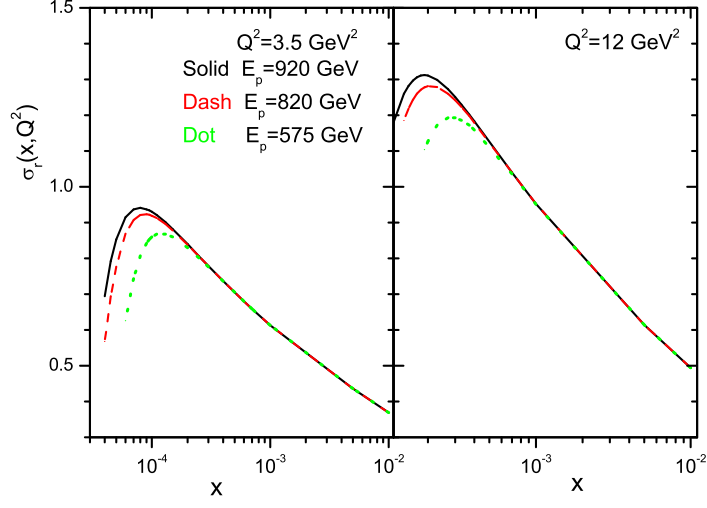


FIG. 7: The NNLO predictions for $\sigma_r(x, Q^2)$ but for different proton beam energies E_p at $Q^2 = 3.5$ and 12 GeV^2 . Notice that the curves terminate when $y = 1$.

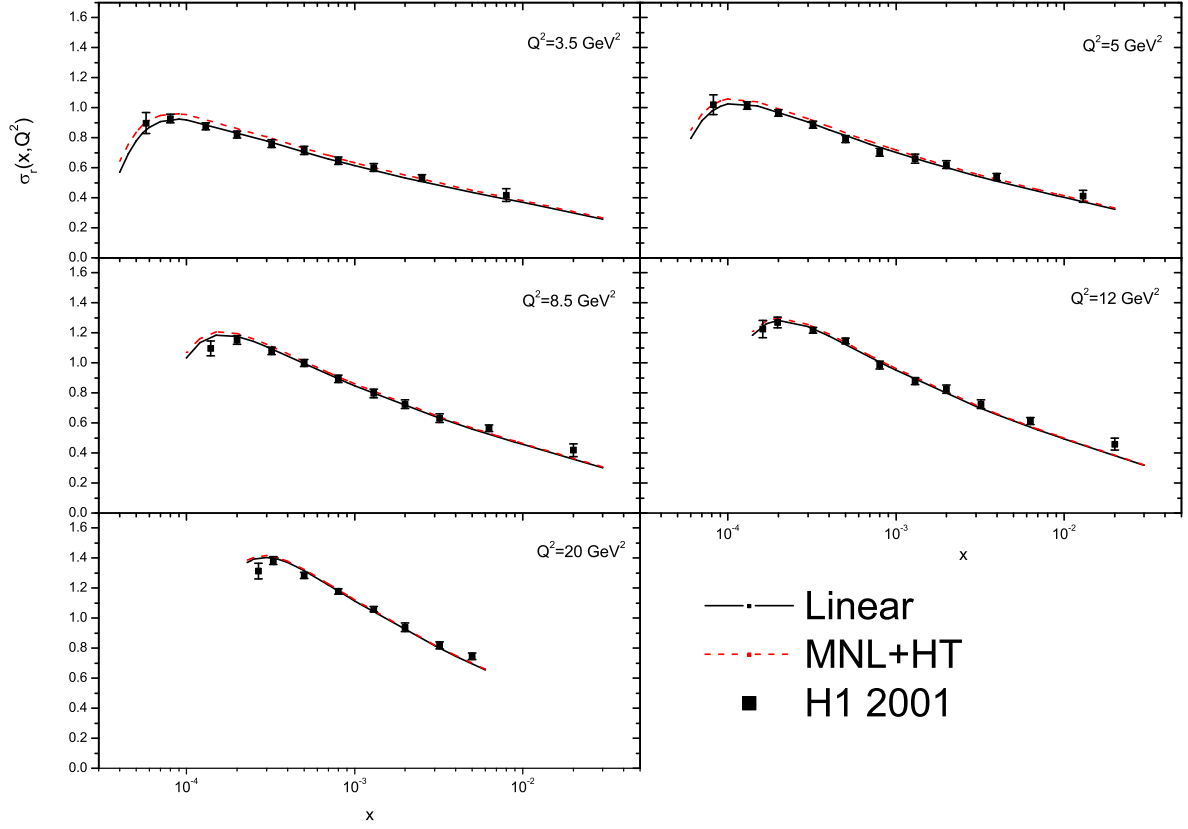


FIG. 8: The NNLO predictions for the reduced DIS cross section. The modified nonlinear (MNL) and higher twist (HT) corrections represent our results at NNLO. The H1 data for some representative fixed values of Q^2 are taken from [42].

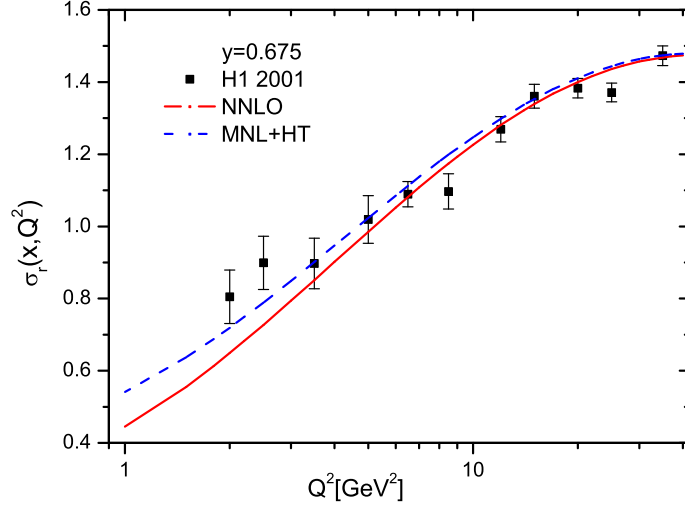


FIG. 9: The NNLO predictions for the reduced DIS cross section at high inelasticity available. The H1 data for some representative fixed values of Q^2 are taken from [42] as accompanied with total errors. Modified nonlinear and higher twist corrections compared with linear results in a wide range of Q^2 .